ACS OMEGA

http://pubs.acs.org/journal/acsodf

Article

Preparation, Characterization, and In Vitro Evaluation of Inclusion Complexes Formed between *S*-Allylcysteine and Cyclodextrins

Rino Tachikawa, Hiroki Saito, Hajime Moteki, Mitsutoshi Kimura, Hiroaki Kitagishi, Florencio Arce, Jr., Gerard Lee See, Takashi Tanikawa, and Yutaka Inoue*

Cite This: *ACS Omega* 2022, 7, 31233−31245

Read Online

ACCESS | Metrics & More | Article Recommendations | Supporting Information

ABSTRACT: The present study prepared inclusion complexes of *S*-allylcysteine (SAC) and cyclodextrin (α, β, γ) by the freeze-drying (FD) method and verified the inclusion behavior of the solid dispersion. Also, the study investigated the effect of SAC/CD complex formation on liver tumor cells. Isothermal titration calorimetry (ITC) measurements confirmed the exothermic titration curve for SAC/αCD, suggesting a molar ratio of SAC/αCD = 1/1, but no exothermic/endothermic reaction was obtained for the SAC/βCD and SAC/γCD system. Powder X-ray diffraction (PXRD) results showed that the characteristic diffraction peaks of SAC and CDs disappeared in FD (SAC/αCD) and FD (SAC/γCD), indicated by a halo pattern. On the other hand, diffraction peaks originating from SAC and βCDs were observed in FD (SAC/βCD). Near-infrared (NIR) absorption spectroscopy results showed that CH and OH groups derived from SAC and OH groups derived from αCD and γCD cavity were shifted, suggesting complex formation due to intermolecular interactions occurring in SAC/αCD and SAC/γCD. Stability test results showed that the stability was maintained with FD (SAC/αCD) over FD (SAC/βCD) and FD (SAC/γCD). In ^{1}H−^{1}H of NOESY NMR measurement, FD (SAC/αCD) was confirmed to have a cross peak at the CH group of the alkene of SAC and the proton (H-3, -5, -6) in the αCD cavity. In FD (SAC/γCD), a cross peak was confirmed at the alkyl group on the carbonyl group side of SAC and the proton (H-3) in the cavity of γCD. From the above, it was suggested that the inclusion mode of SAC is different on FD (SAC/CDs). The results of the hepatocyte proliferation inhibition test using HepG2 cells showed that FD (SAC/βCD) inhibited cell proliferation. On the other hand, FD (SAC/αCD) and FD (SAC/γCD) did not show a significant decrease in the number of viable cells. These results suggest that the difference in the inclusion mode may contribute to the stability and cell proliferation inhibition.

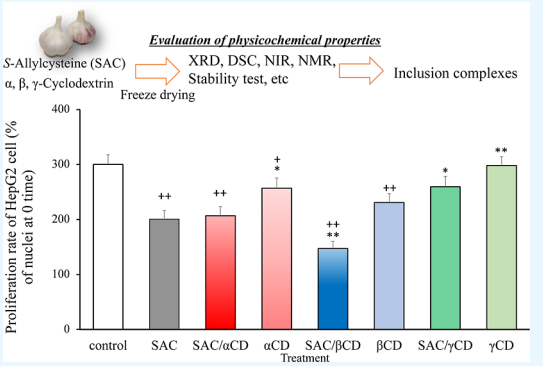

INTRODUCTION

S-Allylcysteine (SAC) is a water-soluble amino acid that is commonly found in aged garlic extract and derived from the catabolism of γ-glutamyl-SAC.[1] SAC is used as a health supplement for its tonic effect. It is purported to have various physiological effects such as antioxidant action,[2] prevention effect against dementia,[3] arteriosclerosis prevention,[4] anticancer effect,[5] and liver damage prevention effect.[6] Garlic is known to contain various constituents including allicin and SAC, and it has been reported that SAC is safer than allicin,[7] and thus, greater utility is expected of SAC. As a component of garlic, SAC has a characteristic garlic odor. Apart from addressing the characteristic garlic odor, it is desirable to enhance the hepatoprotective activity of SAC a characteristic function of SAC from the perspective of nutrition therapy.

Cyclodextrin (CD) is a cyclic polysaccharide, wherein D-glucopyranose is linked by the α-1,4 glycosidic bond. CDs containing 6, 7, and 8 molecules of D-glucopyranose are classified as α-cyclodextrin (αCD), β-cyclodextrin (βCD), and γ-cyclodextrin (γCD), respectively.[8] It has been safely used in various fields such as foods, pharmaceuticals, and cosmetics manufacture.[9] Structurally, CDs have a ring cavity that allows hosting of guest molecules to form inclusion complexes. Inclusion complex formation of *trans*-anethole (AT) and βCD has been reported to improve the stability of the guest molecules.[10] The use of γCD with ferulic acid derivative to form complexes has improved solubility of several model drugs.[11] Furthermore, the formation of catechin with βCD has been reported to enhance the antioxidant activity of catechin.[12]

Various methods are known for the preparation of inclusion complexes, including freeze-drying (FD),[13] coprecipitation,[14] ground mixture,[15] and kneading.[16] In the FD method, the drug solution is frozen and the solvent is sublimed to obtain the

Received: June 4, 2022
Accepted: August 10, 2022
Published: August 24, 2022

complex. For example, the formation of carvacrol/βCD inclusion complexes by the FD method has been shown to improve drug stability, and antibacterial and antioxidant activities.[17] In addition, our previous work has reported the formation of inclusion complexes of caffeic acid (CA) and CDs by FD that resulted in the improvement of CA solubility and antioxidant capacity.[18]

The characteristics of SAC when used alone may be different from those of the SAC/CD inclusion complexes. In other words, it will be interesting to unravel how SAC/CD inclusion complexes would affect the hepato-protective effects of SAC. Thus, enhancement of the hepatoprotective function of SAC through inclusion complex formation could contribute to a new approach to drug format selection for liver diseases. The purpose of this study was to prepare solid dispersions of SAC and CDs (αCD, βCD, and γCD) using the FD method to verify the inclusion behavior of the solid dispersions and to investigate the effect of SAC/CDs complex formation on liver tumor cells.

RESULTS AND DISCUSSION

Determination of Inclusion Molar Ratio between SAC and α, β, γCD. Isothermal titration calorimetry (ITC) measurements were performed to determine the molar ratios of the inclusion complexes of SAC/αCD, SAC/βCD, and SAC/γCD (Figures 1−3). In SAC/αCD, an exothermic reaction was confirmed from the isothermal titration curve. The curve fitting analysis revealed that the binding constant

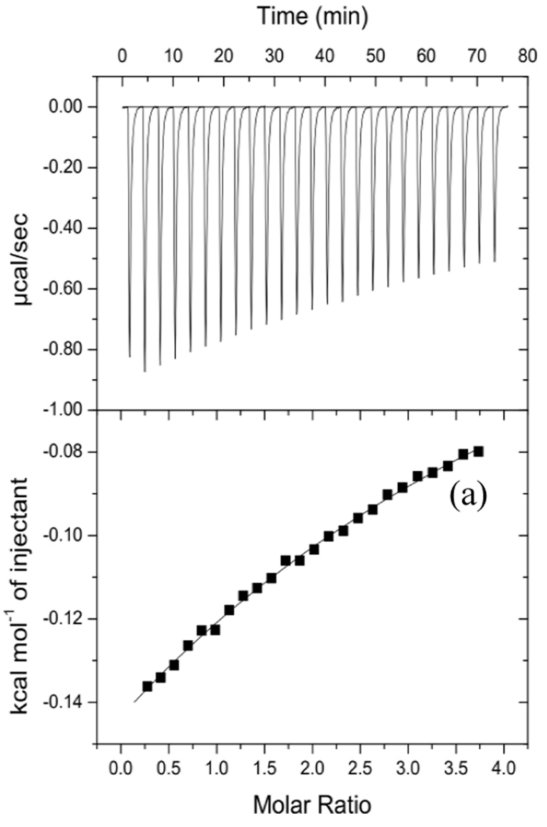

Figure 1. ITC curves of SAC/αCD. The solution (1.4 mL) of CDs (1 mM) dissolved in 0.05 M phosphate buffer were titrated with SAC solution (20 mM) in the same buffer. The solid line in (a) represents the best-fit theoretical curve to determine thermodynamic parameters for this complexation using the ORIGIN software.

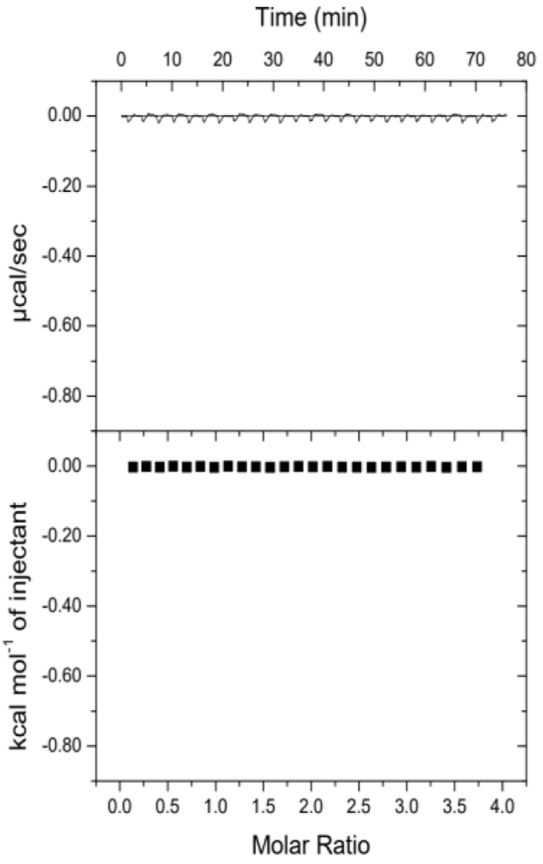

Figure 2. ITC curves of SAC/βCD systems.

(*K*) was 44 M^{-1} with enthalpy (Δ*H*) and entropy changes (Δ*S*) being −14.0 kJ/mol and −15.6 J/mol K, respectively (Figure 1). Because the titration curve was well fitted by an equation based on 1/1 complexation, we conclude that SAC/αCD formed a complex with a molar ratio of 1/1. On the other hand, no significant endothermic/exothermic reaction could not be observed when the SAC solution was titrated by βCD and γCD. In other words, it was presumed that SAC is not easily encapsulated in the β and γ CD cavities (Figures 2 and 3). From the ITC experiments, SAC can be well included in the cavity of αCD in aqueous solution.

Confirmation of FD Product Content. Although the interaction was confirmed only with FD(SAC/αCD) in solution, solid dispersions of αCD, βCD, and γCD with a molar ratio of (SAC/CDs = 1/1) were prepared by FD and evaluated in its solid-state. To examine the content of SAC in the prepared FD product, SAC was quantified by HPLC. From the results, the content was confirmed to be 99.9% for FD (SAC/αCD), 99.7% for FD (SAC/βCD), and 99.9% for FD (SAC/γCD) (Table 1). Therefore, SAC remained stable when prepared by FD, so the physicochemical properties in the solid state were evaluated.

Powder X-ray Diffraction. The ITC results showed the possibility of an inclusion complex with a molar ratio of 1/1 in SAC/αCD. Therefore, SAC/αCD, SAC/βCD, and SAC/γCD were prepared by the FD method, and powder X-ray diffraction (PXRD) measurement was performed to examine the changes in the crystal state (Figure 4).

Characteristic diffraction peaks derived from SAC were observed at 2θ = 5.3 and 33.0° (Figure 4a). Diffraction peaks (2θ = 5.2 and 32.9°) were confirmed with FD SAC alone

https://doi.org/10.1021/acsomega.2c03489
ACS Omega 2022, 7, 31233−31245

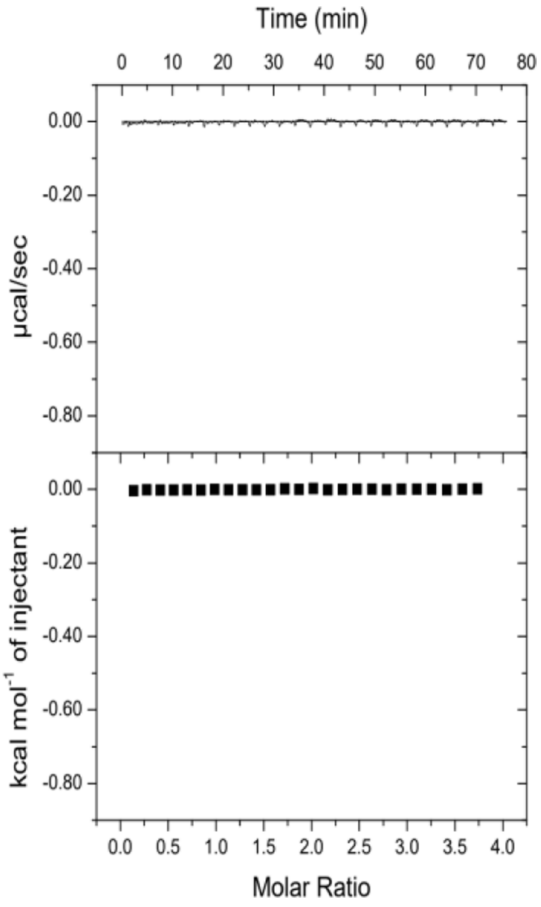

Figure 3. ITC curves of SAC/γCD systems.

Table 1. Change in NIR Absorption Spectra of FD SAC/CD Systems

samples	−CH			−OH	
SAC	4424, 4264				7434
αCD		4338	4975	7194	
PM (SAC/αCD)	4424, 4264	4338	4975	7194	7434
FD (SAC/αCD)	4464, broaden	broaden	4987	7168	7434
βCD		4484	4962	7246	
PM (SAC/βCD)	4424, 4264	4484	4962	7246	7434
FD (SAC/βCD)	4434, broaden	4434	4962	broaden	7434
γCD		4474	4950	7246	
PM (SAC/γCD)	4424, 4264	4474	4950	7246	7434
FD (SAC/γCD)	4454, broaden	4454	4987	7142	7462

(Figure S1a). Diffraction peaks (2θ = 11.8 and 14.2°) were confirmed with αCD alone (Figure 4b), and a halo pattern was observed with FD αCD alone (Figure S1b).

In PM (SAC/αCD), diffraction peaks derived from SAC were confirmed at 2θ = 5.3 and 32.8°, and from αCD at 2θ = 12.0 and 14.2° (Figure 4c). On the other hand, FD (SAC/αCD) exhibited a halo pattern (Figure 4d). Diffraction peak characteristics of 2θ = 6.1, 10.4, 12.3, and 15.2° were confirmed with βCD alone (Figure 4e), and peaks were confirmed at 2θ = 12.5° with FD βCD alone (Figure S1c).

In PM (SAC/βCD), diffraction peaks derived from SAC were confirmed at 2θ = 5.3, 32.8°, and diffraction peaks derived from βCD were confirmed at 2θ = 6.1, 10.4, 12.4, and 15.2° (Figure 4f). On the other hand, for FD (SAC/βCD), the diffraction peak derived from SAC was observed at 2θ = 5.3°, and the diffraction peak derived from βCD was confirmed at 2θ = 10.4, 12.5, and 15.4° (Figure 4g). A characteristic diffraction peak was confirmed at 2θ = 13.9 and 16.4° with γCD alone (Figure 4h), and a halo pattern was observed with FD γCD alone (Figure S1d).

In PM (SAC/γCD), diffraction peaks derived from SAC were confirmed at 2θ = 5.3 and 33.0°, and diffraction peaks derived from γCD were confirmed at 2θ = 14.0 and 16.5° (Figure 4i). On the other hand, FD (SAC/γCD) exhibited a halo pattern (Figure 4j).

It has been reported that PXRD measurements suggest the possibility of inclusion complex formation between CD and guest molecules when peak disappearance or amorphous state is observed in the solid dispersion of CD and guest molecules.[19] The characteristic diffraction peaks of SAC disappeared in FD (SAC/αCD) and FD (SAC/γCD), suggesting that the crystalline state was changed by FD and SAC was encapsulated in the cavities of the CDs. On the other hand, in FD (SAC/βCD), the characteristic diffraction peak of SAC was observed, indicating that SAC is not encapsulated in the cavity of βCD in the solid-state.

Differential Scanning Calorimetry. The changes in the solid-state were observed in the FDs (SAC/CDs) from the results of PXRD measurements. Therefore, differential scanning calorimetry (DSC) measurements were performed to confirm the thermal behavior of each FDs in the solid-state (Figure 5). In SAC alone, an endothermic peak due to dehydration was confirmed at around 56 °C, and an endothermic peak due to melting was confirmed at around 229 °C (Figure 5a). In addition, an endothermic peak due to dehydration was confirmed at 42 °C and an endothermic peak due to melting was confirmed at around 226 °C with FD SAC alone (Figure S2a).

In αCD, an endothermic peak due to dehydration was confirmed at around 70 °C, and an endothermic peak due to decomposition was confirmed at around 290 °C (Figure 5b). In PM (SAC/αCD), an endothermic peak derived from αCD was observed at around 71 °C, a peak of decomposition was observed at 277 °C, and an endothermic peak derived from SAC was confirmed at around 226 °C (Figure 5c). On the other hand, in FD (SAC/αCD), the disappearance of the endothermic peak derived from SAC was confirmed (Figure 5d).

In βCD, an endothermic peak due to dehydration was confirmed at around 106 °C, and an endothermic peak due to decomposition was observed at 297 °C (Figure 5e). In PM (SAC/βCD), an endothermic peak derived from βCD was observed at around 110 °C, an endothermic peak due to decomposition was observed at 277 °C, and an endothermic peak derived from SAC was confirmed at around 216 °C (Figure 5f). In FD (SAC/βCD), an endothermic peak derived from SAC was observed at 174 °C (Figure 5g).

In γCD, an endothermic peak due to dehydration was confirmed at around 103 °C, and an endothermic peak due to decomposition was observed at 292 °C (Figure 5h). In PM (SAC/γCD), an endothermic peak derived from γCD was observed around 89 °C, an endothermic peak due to decomposition was observed around 280 °C, and an

https://doi.org/10.1021/acsomega.2c03489
ACS Omega 2022, 7, 31233−31245

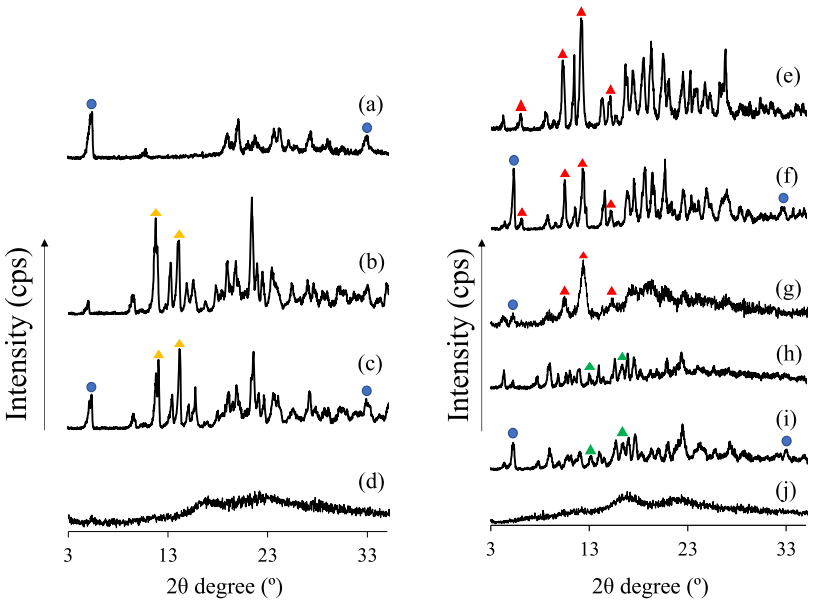

Figure 4. PXRD pattens of SAC intact, SAC/αCD, SAC/βCD, and SAC/γCD systems. (a) SAC intact, (b) αCD intact, (c) PM (SAC/αCD = 1/1), (d) FD (SAC/αCD = 1/1), (e) βCD intact , (f) PM (SAC/βCD = 1/1), (g) FD (SAC/βCD = 1/1), (h) γCD intact, (i) PM (SAC/γCD = 1/1), and (j) FD (SAC/γCD = 1/1).

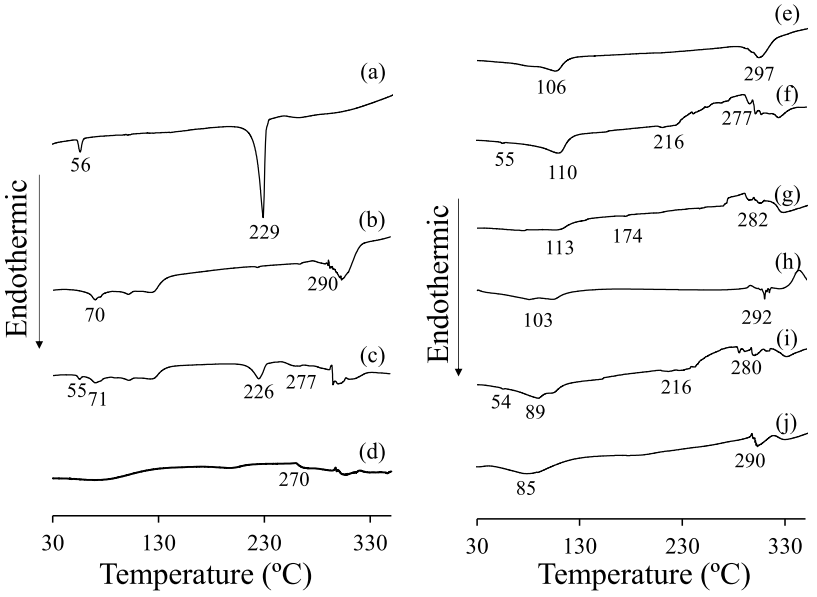

Figure 5. DSC curves of SAC intact, SAC/αCD, and SAC/βCD SAC/γCD systems. (a) SAC intact, (b) αCD intact, (c) PM (SAC/αCD = 1/1), (d) FD (SAC/αCD = 1/1), (e) βCD intact , (f) PM (SAC/βCD = 1/1), (g) FD (SAC/βCD = 1/1), (h) γCD intact, (i) PM (SAC/γCD = 1/1), and (j) FD (SAC/γCD = 1/1).

endothermic peak derived from SAC was confirmed around 216 °C (Figure 5i). On the other hand, in FD (SAC/γCD), the disappearance of the endothermic peak derived from SAC was confirmed (Figure 5j). Typically, the crystal lattice of a guest molecule changes its melting point and boiling point due to the formation of an inclusion complex, and DSC measurements observe the disappearance of endothermic peaks, the appearance of new peaks, and the spread of peaks.[20] For example, DSC measurements with the coprecipitate of Cyclamen aldehyde (Cya) and βCD have reported that the sublimation/decomposition points of Cya disappeared in CP (Cya/βCD).[21] Therefore, the endothermic peaks of FD (SAC/αCD) and FD (SAC/γCD) disappeared, suggesting the formation of an inclusion complex.

NIR Spectroscopy. The formation of inclusion complexes of solid dispersions prepared by FD was confirmed by PXRD and DSC measurements. On the other hand, it was initially suggested by ITC analysis that only SAC/αCD demonstrated molecular interactions. Near-infrared (NIR) absorption spectra were recorded to confirm intramolecular interactions in SAC/CDs (Figures 6−8) (Table 1). In intact SAC samples, the CH group was confirmed at 4424 and 4264 cm^{-1}. In PM SAC/αCD, the CH group from SAC was confirmed at 4424 and 4264 cm^{-1}, and a peak of the CH group derived from αCD was observed at 4338 cm^{-1}. The OH group derived from αCD

https://doi.org/10.1021/acsomega.2c03489
ACS Omega 2022, 7, 31233−31245

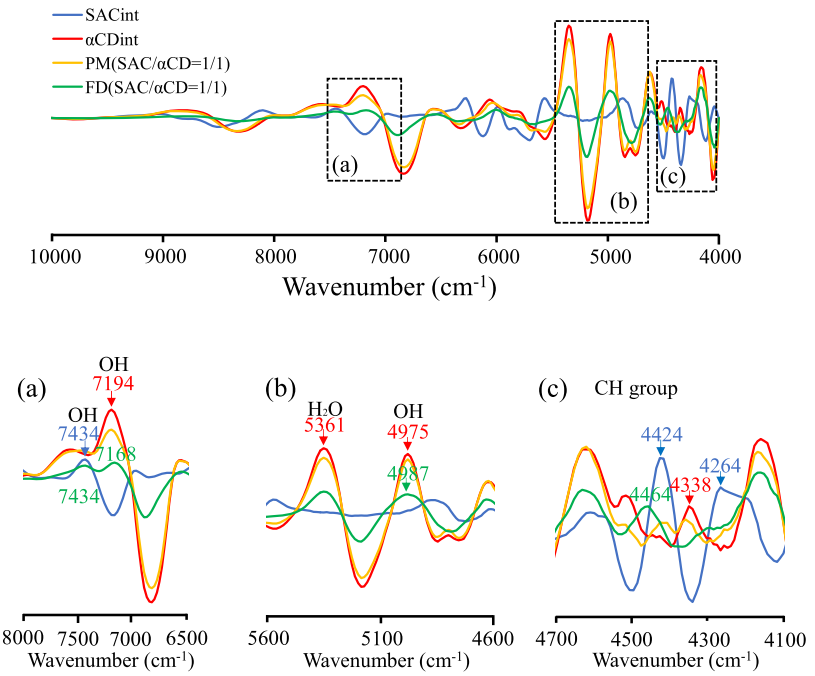

Figure 6. Second differentiation NIR absorption spectra of FD SAC/αCD = 1/1 system. (a) 8000−6500, (b) 5600−4600, and (c) 4700−4100 cm^{-1}.

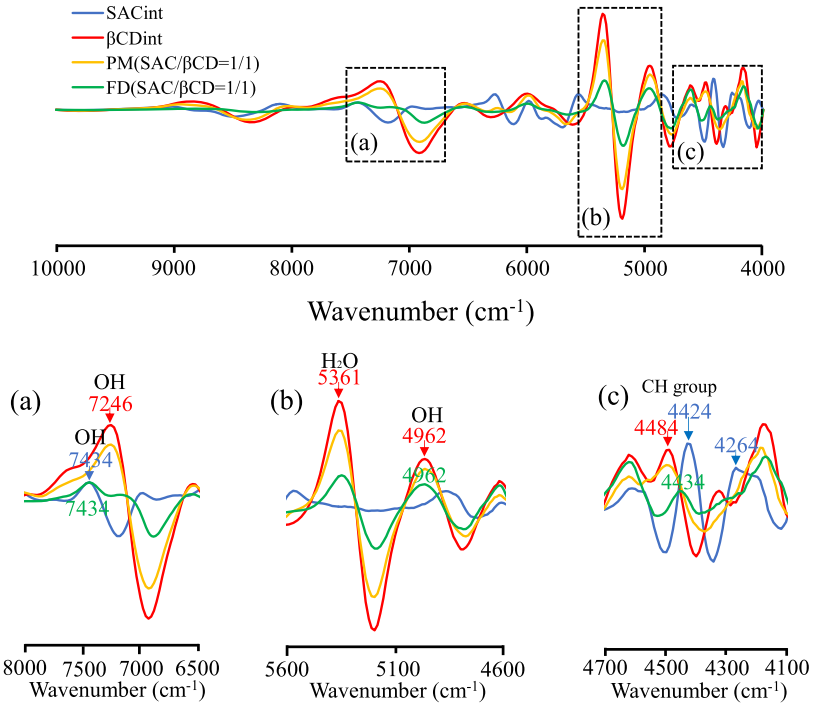

Figure 7. Second differentiation NIR absorption spectra of FD SAC/βCD = 1/1 system. (a) 8000−6500, (b) 5600−4600, and (c) 4700−4100 cm^{-1}.

was confirmed at 7194 cm^{-1}. In FD (SAC/αCD), it was confirmed that the CH group of 4424 cm^{-1} alkene peak-shifted to 4464 cm^{-1} and the peak of 4264 cm^{-1} was broadened. In addition, a peak of the CH group derived from αCD alone was observed at 4338 cm^{-1}; however, FD (SAC/αCD) showed broadening (Figure 6c). A peak of OH groups from the αCD cavity was observed at 4975 cm^{-1}, while in FD (SAC/αCD), the peak from the same OH was confirmed to have shifted to 4987 cm^{-1} (Figure 6b). In addition, another OH group originating from αCD was identified at 7194 cm^{-1}, and the peak shift in FD (SAC/αCD) was confirmed at 7168 cm^{-1}. Furthermore, the peak of the OH group derived from SAC was confirmed at 7434 cm^{-1}, and the peak of FD (SAC/αCD) was confirmed at 7434 cm^{-1} (Figure 6a). From the above, it was suggested that an intramolecular interaction was formed between the alkyl group of SAC and the OH group in the αCD cavity.

https://doi.org/10.1021/acsomega.2c03489
ACS Omega 2022, 7, 31233−31245

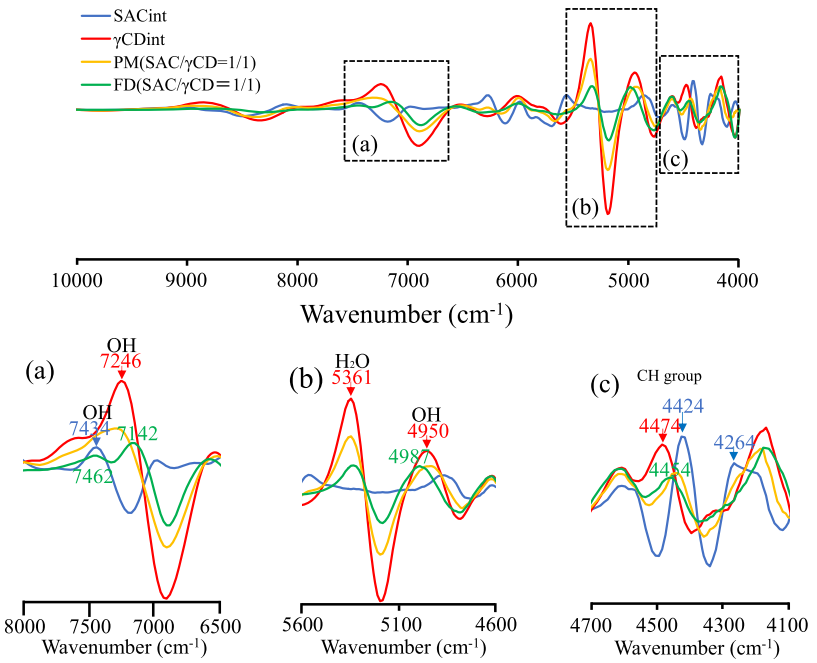

Figure 8. Second differentiation NIR absorption spectra of FD SAC/γCD = 1/1 system. (a) 8000−6500, (b) 5500−4600, and (c) 4700−4100 cm^{-1}.

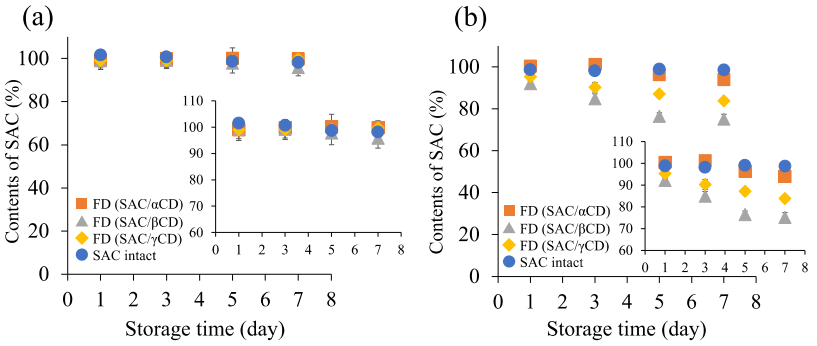

Figure 9. Changes in SAC content after storage under vacuum conditions at temperatures of 40 and 80 °C. Each point presents the mean ± SD (n = 3). (a) Under 40 °C conditions. (b) Under 80 °C conditions.

In SAC/βCD, peaks derived from the CH group only for SAC were confirmed at 4424 and 4264 cm^{-1}, and similar peaks were confirmed for FD SAC alone. In PM SAC/βCD, the CH group only for SAC was confirmed at 4424 and 4264 cm^{-1}, and a peak of the CH group derived from βCD was observed at 4484 cm^{-1}. The OH group derived from βCD was confirmed at 7246 cm^{-1}. In FD (SAC/βCD), it was confirmed that the CH group of the 4424 cm^{-1} alkene peak shifted to 4434 cm^{-1} and at broadened peak 4264 cm^{-1}. In addition, the peak of the CH group derived from βCD was found at 4484 cm^{-1}, and the peak shifted to 4434 cm^{-1} in FD (SAC/βCD) (Figure 7c). A peak of the OH group derived from the βCD cavity was observed at 4962 cm^{-1}, and a similar peak was confirmed in FD (SAC/βCD) (Figure 7b). However, βCD-derived OH groups were confirmed at 7246 cm^{-1}, and FD (SAC/βCD) peak was broadened. The peaks of SAC-derived OH groups and the FD (SAC/βCD) were confirmed at 7434 cm^{-1} (Figure 7a). From the above, it was suggested that an intramolecular interaction was formed between the alkyl group of SAC and the OH group derived from glucose outside of the βCD cavity.

In SAC/γCD, peaks derived from the CH group for SAC only were confirmed at 4424 and 4264 cm^{-1}, and similar peaks were confirmed for FD SAC alone. In PM SAC/γCD, the CH group only for SAC was confirmed at 4424 and 4264 cm^{-1}, and a peak of the CH group derived from γCD was observed at 4474 cm^{-1}. The OH group derived from γCD was confirmed at 7246 cm^{-1}. In FD (SAC/γCD), it was confirmed that the CH group of 4424 cm^{-1} alkene peak-shifted to 4454 cm^{-1} and the peak at 4264 cm^{-1} was broadened. In addition, the peak of the CH group derived from γCD was found at 4474 cm^{-1}, and the peak shifted to 4454 cm^{-1} in FD (SAC/γCD) (Figure 8c). A peak of OH groups from the γCD cavity was observed at 4950 cm^{-1}. On the other hand, it was notable that the peak of FD (SAC/γCD) shifted to 4987 cm^{-1} (Figure 8b). In addition, the OH group derived from γCD was confirmed at 7246 cm^{-1}, and the peak shift of FD (SAC/γCD) was confirmed at 7142 cm^{-1}. Furthermore, the peak of the OH group derived from SAC was confirmed at 7434 cm^{-1}, and the peak of FD (SAC/γCD) was confirmed at 7462 cm^{-1} (Figure 8a). From the above, it was suggested that an intramolecular interaction was formed between the alkyl group derived from the OH group

https://doi.org/10.1021/acsomega.2c03489
ACS Omega 2022, 7, 31233−31245

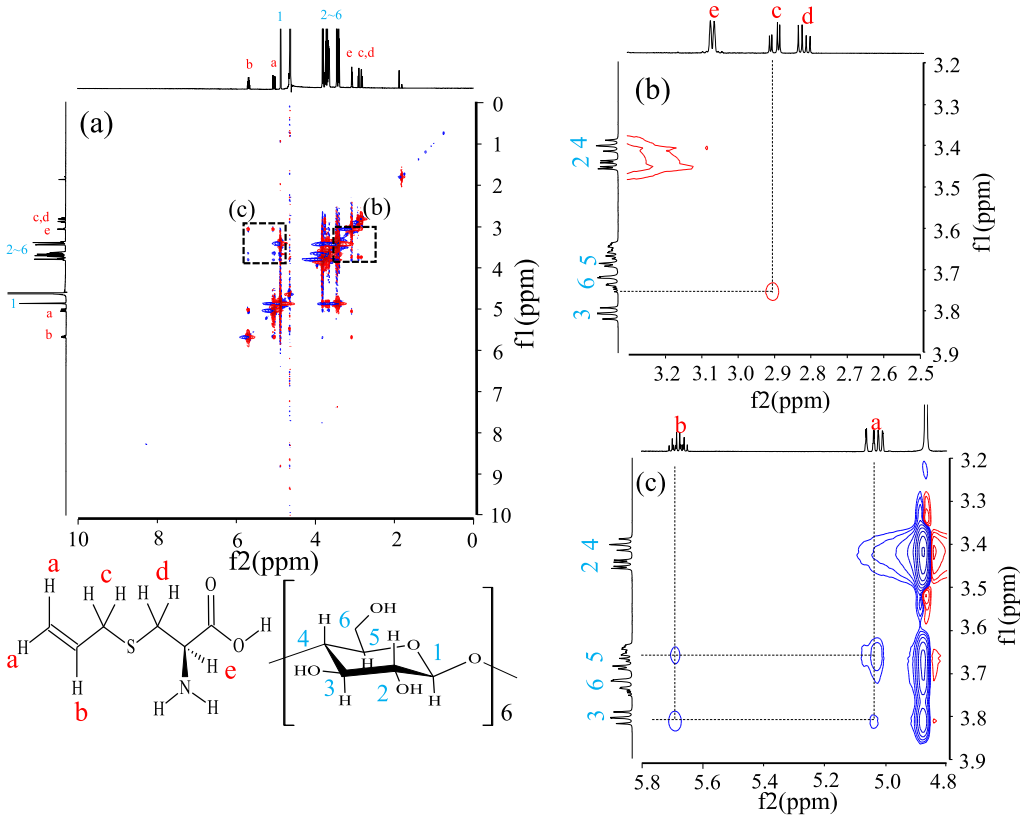

Figure 10. {^{1}H−^{1}H} NOESY NMR spectra of FD (SAC/αCD = 1/1) in D_2O. (a) f1 is 0−10 ppm, f2 is 0−10 ppm. (b) f1 is 3.2−3.9 ppm, f2 is 2.5−3.3 ppm. (c) f1 is 3.2−3.9 ppm, and f2 is 4.8−5.8 ppm.

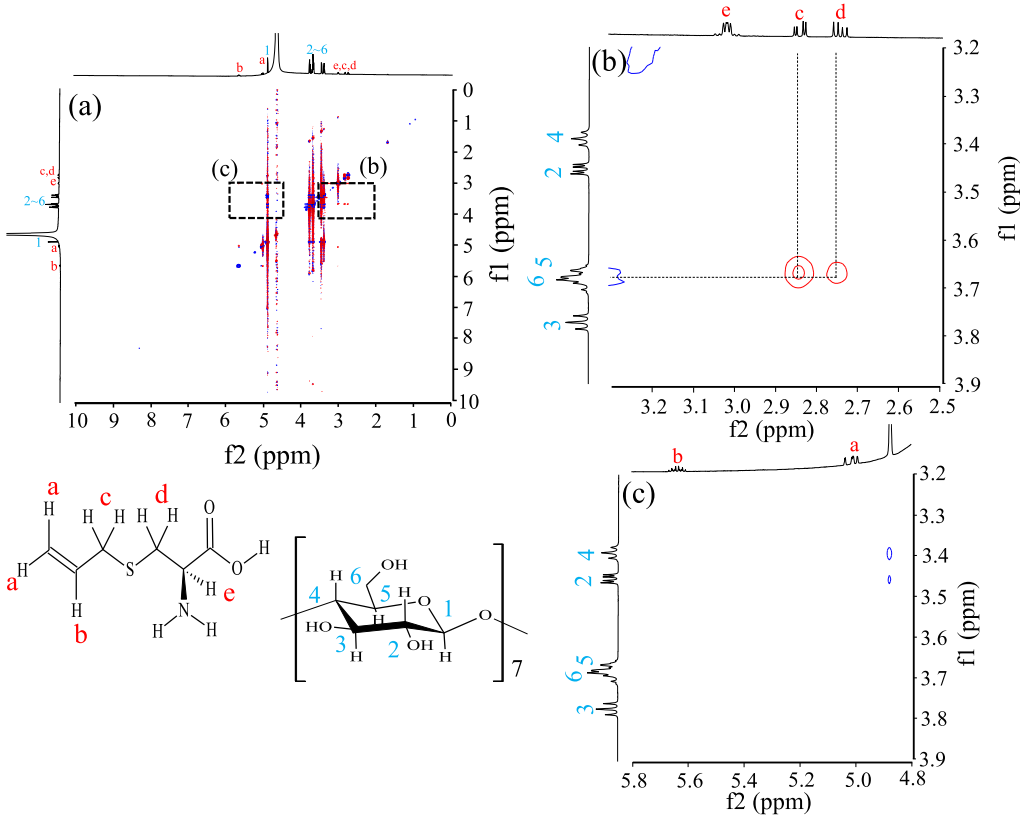

Figure 11. {^{1}H−^{1}H} NOESY NMR spectra of FD (SAC/βCD =1/1) in D_2O. (a) f1 is 0−10 ppm, f2 is 0−10 ppm. (b) f1 is 3.2−3.9 ppm, f2 is 2.5−3.3 ppm. (c) f1 is 3.2−3.9 ppm, and f2 is 4.8−5.8 ppm.

https://doi.org/10.1021/acsomega.2c03489
ACS Omega 2022, 7, 31233−31245

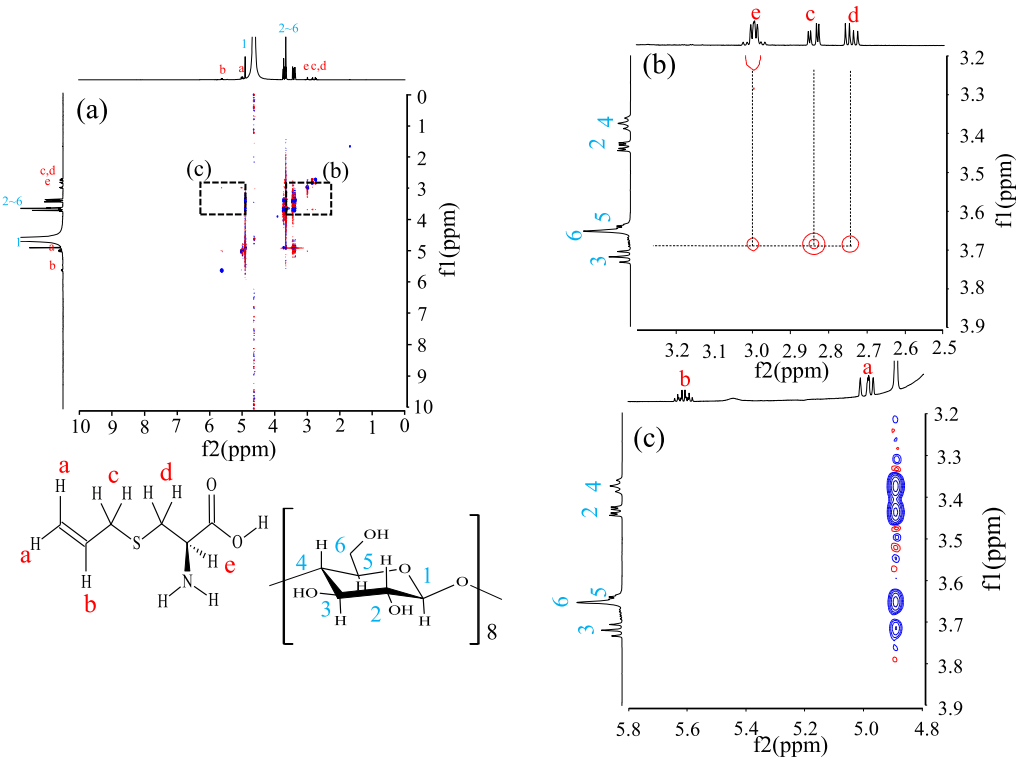

Figure 12. {^{1}H−^{1}H} NOESY NMR spectra of FD (SAC/γCD =1/1) in D_2O. (a) f1 is 0−10 ppm, f2 is 0−10 ppm. (b) f1 is 3.2−3.9 ppm, f2 is 2.5−3.3 ppm. (c) f1 is 3.2−3.9 ppm, and f2 is 4.8−5.8 ppm.

and the carbonyl group of SAC and the OH group in the γCD cavity.

Stability Test. Stability tests of SAC/CDs in their solid-states were performed because it was suggested that FD would form inclusion complexes for SAC/αCD and SAC/γCD in its solid-state. The results of stability tests are shown in Figure 9. There was no significant change observed in the content, as SAC and FD (SAC/CDs), SAC from day 1 to day 7 under the temperature of 40 °C and vacuum drying conditions. Stability of SAC in an aqueous solution at 50 °C for 5 days has been previously recorded.[22] Therefore, higher temperature for stability tests were conducted at 80 °C and under vacuum-drying conditions. On day 1, the SAC content was 98.7%, SAC content in FD (SAC/αCD) was at 100.4%, SAC content in FD (SAC/βCD) was at 92.1%, and SAC content in FD (SAC/γCD) was at 95.3%. On day 7, 98.6% of SAC content was confirmed. On the other hand, FD (SAC/αCD), FD (SAC/βCD), and FD (SAC/γCD) contained 94.0, 75.1, and 83.8% of SAC, respectively. Nguyen and Yoshii developed inclusion complexes with allyl sulfide, which is structurally similar to SAC, and CDs explaining the release behavior of allyl sulfide. They reported that the stability of allyl sulfide/CDs was better in the αCD inclusion complex than in the βCD and γCD inclusion complexes and that the release of allyl sulfide was suppressed in the αCD inclusion complex.[23] It was noted that the exchange of allyl sulfide molecules and water molecules within the CD cavities may be involved.[23] Therefore, the weight loss of SAC in FD (SAC/βCD) and FD (SAC/γCD) may be due to the exchange of water molecules with SAC encapsulated in the CD cavities. In addition, the difference in the diameter of the CDs cavities suggests that the exchange reaction with water molecules is not as likely to occur in αCD, where the cavity diameter is smaller than in βCD and γCD, contributing to the stability of the SAC. This suggests that FD (SAC/CDs) can remain stable at usual room temperatures. NMR measurements were then performed to confirm the inclusion behavior of SAC with CDs.

Measurement of ^{1}H−^{1}H NOESY NMR Spectra. ^{1}H−^{1}H NOESY NMR measurements were performed to investigate the detailed intramolecular interactions of FD (SAC/αCD), FD (SAC/βCD), and FD (SAC/γCD) in solution (Figures 10−12). The ^{1}H−^{1}H NOESY NMR measurement was used to infer the relative position of the inclusion complex because it can confirm the interaction between the guest molecule and the CD cavity.[24] In FD (SAC/αCD), a cross peak was confirmed between the peak Hc (2.90 ppm) derived from the alkyl group (H) of SAC and the peak H-6 (3.75 ppm) derived from αCD (Figure 10b). Furthermore, a cross peak was confirmed between Ha (5.06 ppm) and Hb (5.69 ppm) of SAC and H-3 (3.81 ppm) and H-5 (3.66 ppm) derived from αCD (Figure 10c). It is generally known that H-3 is a proton present at the wide edge of the CD ring and H-6 is a proton present at the narrow edge of the CD ring.[25] From the above, it was inferred that in FD (SAC/αCD), SAC is encapsulated from the protons of the H-a, -b, and -c portions of SAC from the narrow edge to the wide edge of αCD. The expected inclusion mode of FD (SAC/αCD) is shown in Scheme 1.

In FD (SAC/βCD), a cross peak was confirmed between H-c (2.84 ppm) and H-d (2.75 ppm) of SAC and H-6 (3.68 ppm) of βCD, revealing a slight interaction with the rim of βCD (Figure 11b). In ^{1}H−^{1}H NOESY NMR measurements of FD (SAC/βCD), cross-peaks have been identified but ITC, PXRD, DSC, and NIR results indicate that SAC is not encapsulated in the βCD cavity suggesting that it touches only the narrower rim of βCD. Because the interaction is shown at the rim of βCD (H-6), it is believed that H-c and H-d of SAC

https://doi.org/10.1021/acsomega.2c03489
ACS Omega 2022, 7, 31233−31245

Scheme 1. Proposed Structure Images of SAC/αCD Complexes

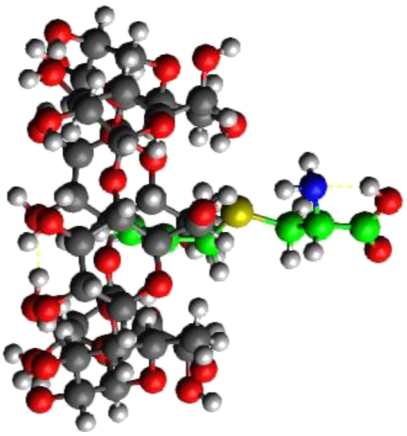

are in contact with the exposed part of the outer cavity of the βCD. The expected inclusion mode that may be found in FD (SAC/βCD) is shown in Scheme 2.

Scheme 2. Proposed Structure Images of SAC/βCD Complexes

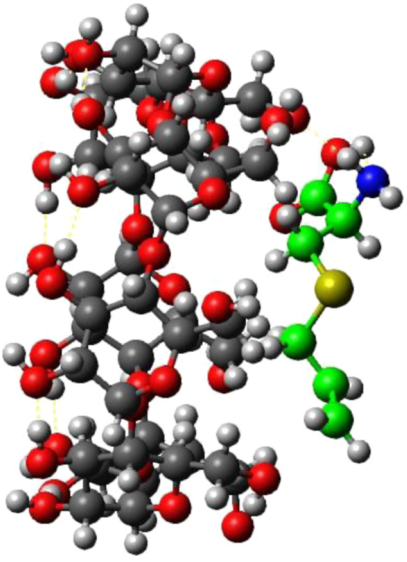

Interestingly, in FD (SAC/γCD), between He (2.99 ppm), Hc (2.86, 2.83 ppm), and Hd (2.74 ppm) of SAC and H-3 (3.70 ppm) in the γCD cavity, a cross peak was confirmed (Figure 12b). From this, it can be inferred that in FD (SAC/γCD), the protons of H-c, -d, and -e of SAC are encapsulated from the wide edge to the narrow edge of γCD. The expected inclusion mode in the FD (SAC/γCD) is shown in Scheme 3. This suggests that FD (SAC/αCD) and FD (SAC/γCD) are formed as inclusion complexes. It was suggested that FD (SAC/αCD) was encapsulated in the double bond moiety of SAC, and FD (SAC/γCD) was encapsulated from the carbonyl group to the thiol group moiety of cysteine. Therefore, different inclusion styles were demonstrated for inclusion complexes. Schemes 1−3 are structures not obtained by energy calculations using computational methods.

This result does not necessarily indicate the presence or absence of inclusion complex formation, but rather that some drugs may form inclusion complexes depending on the choice

Scheme 3. Proposed Structure Images of SAC/γCD Complexes

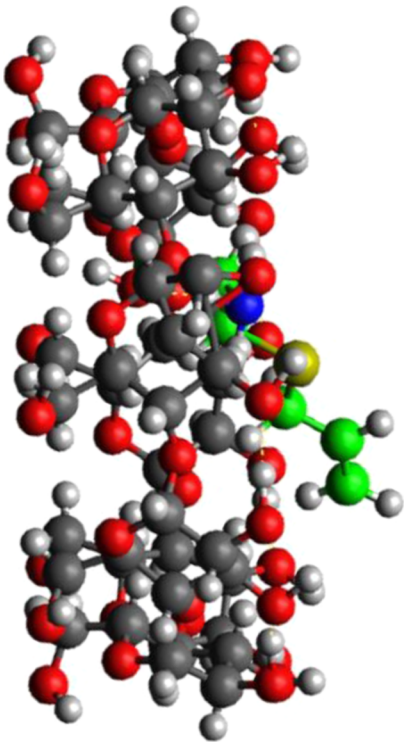

of preparation method (i.e., FD method in this study). In other words, we believe that it is important to combine the chemical analysis of both the solid state and liquid states.

Cell Proliferation Suppression Test. The results have shown that FDs (SAC/CDs) possess different inclusion modes depending on the kind of CDs employed. SAC has been reported to have hepatoprotective effects.[26] Therefore, to investigate the effect of the various SAC/CDs inclusion complex prepared in this study on the liver cells, we performed a hepatocyte proliferation inhibition assay using HepG2 cells (Figure 13). In this test, SAC exhibited approximately 16 and 33% reduction in viable cell counts at concentrations of 10^{-7} and 10^{-6} M, respectively. Interestingly, when FD (SAC/βCD) was applied at the same concentrations, it resulted in a decrease of about 30 and 45%, respectively. Inhibitory activity of FD (SAC/αCD) and FD (SAC/γCD) were comparable to SAC and showed no significant decrease. The effect of pure α, β, and γCDs on HepG2 cells were also performed but no significant decrease was observed for α and γCDs. On the other hand, a decrease of about 15% was observed for βCDs. A study involving βCD/glycyrrhizin acid reported a similar finding wherein inhibition of cell proliferation via the mitochondrial dysfunction pathway in HepG2 cells was observed.[27] Organosulfur compounds such as SAC have been reported to have anticancer activity by promoting mitotic arrest and inducing apoptosis through covalent binding to tubulin via thiol−disulfide exchange reaction with thiol groups.[28] In addition, NMR results showed that FD (SAC/βCD) has a unique complex formation wherein SAC was not encapsulated in the CD cavity and a portion of SAC interacts with H-6 in the CD. The complex is formed by the interaction of a portion of SAC with H-6 of CD. The complex is suggested to be formed by the exposure of the thiol group of SAC (Scheme 2). This suggests that the inhibition of cell

https://doi.org/10.1021/acsomega.2c03489
ACS Omega 2022, 7, 31233−31245

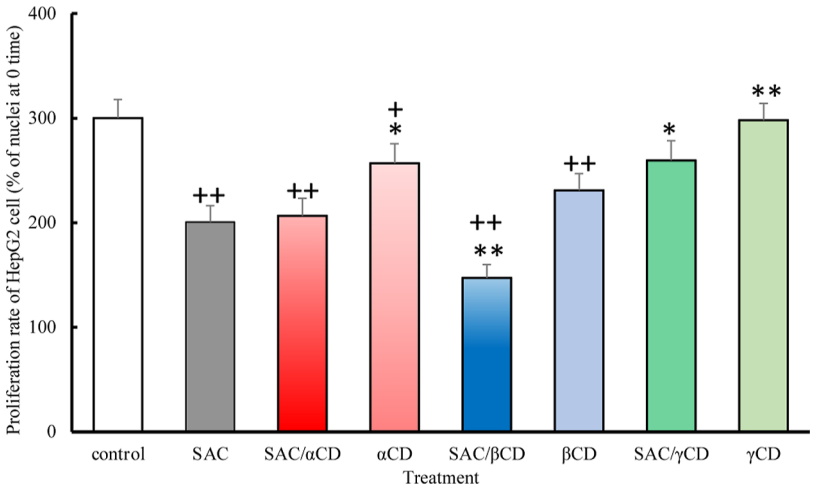

Figure 13. Inhibitory effects of SAC and/or α,β,γ-cyclodextrins on the growth of HepG2 cells. Cells were plated at 2×10^5 cell/well with 3% FCS in DMEM, and after a 24 h attachment period, cells were cultured in serum-free medium containing 10^{-6} M SAC with or without α,β,γ-cyclodextrins (SAC intact, SAC/αCD, αCD intact, SAC/βCD, βCD intact, SAC/γCD, or γCD intact), and the number of nuclei (cell proliferation) were measured 48 h after the addition of SAC/α,β,γ-cyclodextrins. Values are shown as means ± S.E.M. ($N = 3$, Tukey's test). *($p < 0.05$), **($p < 0.01$) shows comparison with SAC intact, +($p < 0.05$), ++($p < 0.01$) shows comparison with control.

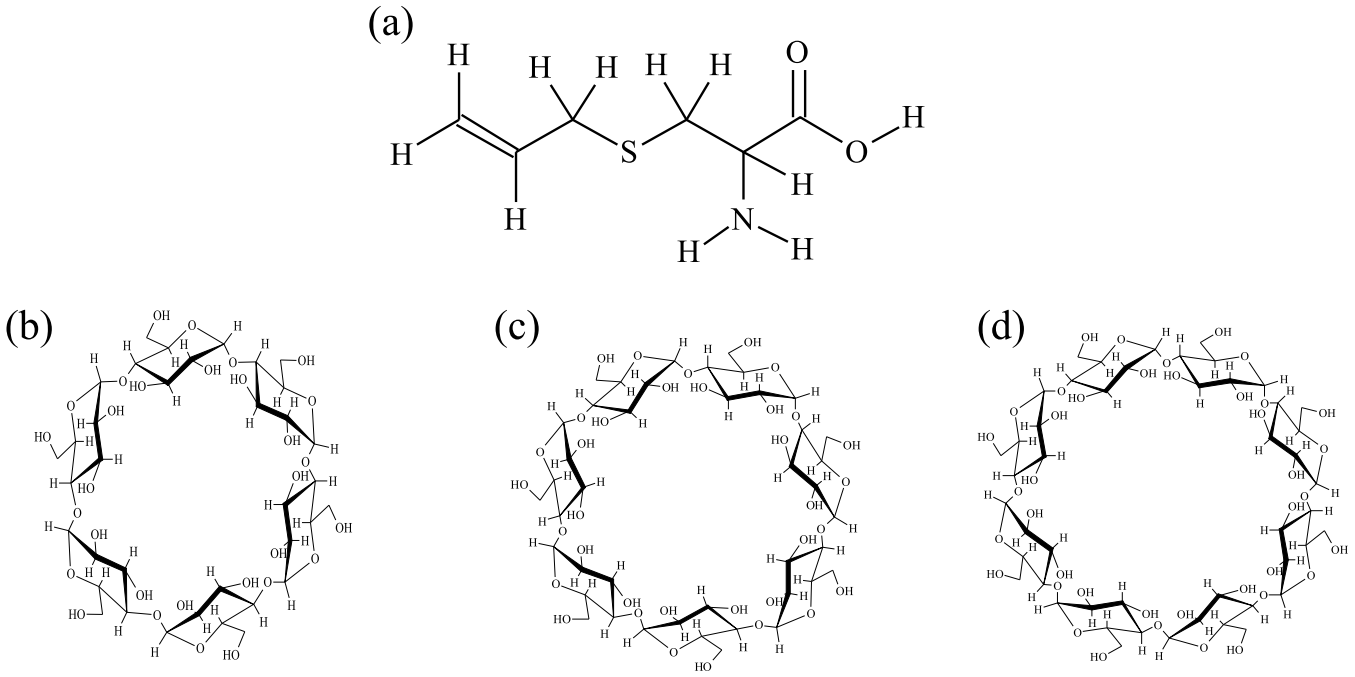

Figure 14. Chemical structures of SAC, CDs. (a) SAC, (b) αCD, (c) βCD, and (d) γCD.

proliferation observed in FD (SAC/βCD) is due to the synergistic effect of the anti-tumor property of βCD and the thiol group of SAC. In addition, βCD is characterized as less soluble in water than α and γCD, which may have affected intake by hepatocytes. Therefore, these suggest that FD (SAC/βCD), in which thiol group is exposed as an inclusion mode of SAC, has a higher anticancer effect on hepatocellular carcinoma.

■ CONCLUSIONS

SAC/αCD and SAC/γCD inclusion complexes were successfully prepared by FD at an inclusion molar ratio of 1/1. SAC in FD (SAC/αCD) remained stable when compared with FD (SAC/βCD) and FD (SAC/γCD) which is attributed to the difference in inclusion form. NMR measurements revealed the different inclusion patterns for the FD SAC/CDs. In the hepatocyte proliferation inhibition assay, FD (SAC/βCD), an inclusion complex with externalized thiol SAC groups, resulted in a higher inhibitory effect on cancer cells. The present study finds an application in drug design, food, and nutrition research involving SAC and garlic-derived biomolecules.

■ MATERIALS AND METHODS

Materials. SAC (≥ 98%) (lot WWHCI-LB) was purchased from Sigma-Aldrich (Figure 14a).

αCD, βCD, and γCD provided by CycloChem Bio Co., Ltd. (Tokyo, Japan) was stored at a temperature of 40 °C and relative humidity of 82% for 7 days. Humidity-controlled

https://doi.org/10.1021/acsomega.2c03489
ACS Omega 2022, 7, 31233−31245

storage was used (Figure 14b−d). Deuterium oxide (D_2O, 99.9%) used as an NMR solvent was purchased from ISOTEC (USA). The other reagents were obtained from Wako Pure Chemical Industries, Ltd. (Tokyo, Japan).

Preparation of Physical Mixture and Lyophilized Product. The physical mixture (PM) was prepared by weighing SAC and α, β, and γCD in a 1:1 molar ratio and mixing them with a vortex mixer for 1 min. For the preparation of the FD product, SAC and α, β, and γCD were weighed in a molar ratio (1/1) to a total volume of 100 mg (SAC/αCD = 13.00/87.00 mg, SAC/βCD = 10.87/89.13 mg, SAC/γCD = 9.63/90.37 mg), thawed in 10 mL of distilled water, and pre-frozen at −30° C. The pre-frozen product was freeze-dried in a freeze-dryer.

METHODS

ITC Measurement. SAC solution (0.3 mL) was placed in a syringe and titrated with approximately 1.4 mL of CD solution in the cell. The heat generated during the titration was continuously recorded. The solvent used was 0.05 M phosphate buffer (pH 7.0). The temperature was set at 25 °C and the heat upon dilution was independently monitored.

The coupling constant is calculated from the slope of the following straight line using eq 1.

$$K = [MX]/[M][X] \quad (1)$$

The Gibbs free energy change (ΔG) can be directly quantified using the ITC measurement to directly determine the binding constant (K) of the interaction, the binding ratio (n) of the reaction, and the change in enthalpy (ΔH). Entropy change (ΔS) can be obtained from eqs 2 and 3. The curve fitting analysis was performed using the ORIGIN software program equipped with MicroCal Isothermal Titration Calorimeter VP-ITC.

$$\Delta G = -RT \ln K \quad (2)$$

$$\Delta G = \Delta H - T\Delta S \quad (3)$$

Quantification of SAC Using HPLC. The quantification of SAC was performed by high-performance liquid chromatography (HPLC: X-LC, JASCO, Tokyo, Japan) at a wavelength of 205 nm. The column used was Inertsil ODS-3 (4.6 × 150 mm, Φ5 μm), the sample injection volume was 50 μL, and the column temperature was 45 °C. For the quantification conditions of SAC, a mixed solution of phosphoric acid (0.1%)/acetonitrile (4/1) was used as the mobile phase, and the retention time was adjusted to 5 min. The SAC quantitation and detection limits were also calculated, with the quantitation limit calculated to be 3.23 μg/mL and the detection limit (DL) calculated to be 1.06 μg/mL.

Powder X-ray Diffraction. The measurement was performed using a powder X-ray diffraction measuring device (Miniflex II, Rigaku corporation, Tokyo). The diffraction intensity was measured using a NaI scintillation counter. For PXRD, Cu rays (30 kV, 15 mA) were used as X-rays. The X-ray diffraction measurement was performed under the conditions of a scan speed of 4°/min, a sampling width of 0.02°, and a measurement range of 2θ = 3−35°. The powder sample was filled in a glass plate so that the sample plane was flat, and the measurement was performed.

Differential Scanning Calorimetry. Themo plus Evo high-sensitivity differential scanning calorimeter (Rigaku Corporation, Tokyo, Japan) was used to identify thermal transitions in the prepared SAC complexes. The samples (2 mg) were filled into an aluminum pan and scanned under a heating range of 30−350 °C at of 5.0 °C/min increments with nitrogen gas at a flow rate of 60 mL/min.

NIR Absorption Spectroscopy. The changes in the molecular interaction of the sample was confirmed using a Fourier transform NIR spectroscope (JASCO V-770, JASCO Corporation, Tokyo, Japan). The conditions were a measured wavenumber of 10 000−4000 cm^{-1}, a measurement time of 8 s, and a measurement temperature of 25 °C. Each sample (3 mg) was filled in a fine powder cell and measurements were taken at intervals of 5 nm in the optical path. Moreover, the obtained spectrum was secondarily differentiated.

Measurement of $^1H-^1H$ NOESY NMR Spectra. The NMR System 700 MHz (Agilent Technologies, Santa Clara, CA, USA) was used. Analysis was carried out using D_2O as the solvent, the resonance frequency was 699.6 MHz, the pulse width was 10.05°, and the relaxation time was at 1.000 ms. The measurement time was about 10 h, and the measurement was performed at 20 °C.

Stability Test. The stability test was performed by storing samples under the conditions of 40 and 80 °C in vacuum. At day 1, 3, 5, and 7 days, the samples were measured for their SAC content using an HPLC system. For the stability test, solid dispersion of FD (SAC/CDs) was stored as a powder.

Hepatocyte Proliferation Test for HepG2. Human hepatoblastoma cell line HepG2 cells (RCB1886) were purchased from the RIKEN BRC through the National Bio-Resource Project of the MEXT (Japan). HepG2 cells were cultured in Dulbecco's modified Eagle medium (DMEM) containing 10% fetal bovine serum, 100 units/mL penicillin, and 100 μg/mL streptomycin in a humidified atmosphere of 5% CO_2 at 37 °C (Knowles. *Science*. **1980,** *209,* 497−499). After the cells adhered and grown to 80% confluence, the culture medium was removed and washed with an appropriate amount of PBS and digested with 0.25% trypsin. Cells in the logarithmic phase of growth were selected for following experiments. Hepatocytes in their logarithmic growth phase were seeded in six-well plates at 1.0×10^5 cells per well and cultured overnight at 37 °C. After a 24 h attachment period, the medium was replaced with a serum-free medium. Reagents added to hepatocytes were SAC or SAC-CD. The cell proliferation effect of SAC or SAC-CD were evaluated by measuring the number of HepG2 nuclei using a method described by Kimura with minor modifications (Kimura EJP. **1997,** *324,* 267−276). Briefly, HepG2 nuclei isolated using 0.1% Triton-X100 containing 0.1 M citric acid and were stained with 0.3% trypan blue, and the number of nuclei was measured by a hemocytometer.

ASSOCIATED CONTENT

Supporting Information

The Supporting Information is available free of charge at https://pubs.acs.org/doi/10.1021/acsomega.2c03489.

PXRD pattens of FD SAC intact, FD αCD intact, FD βCD intact, and FD γCD intact systems and DSC curves of SAC intact, SAC/αCD, and SAC/βCD SAC/γCD systems (PDF)

https://doi.org/10.1021/acsomega.2c03489
ACS Omega 2022, 7, 31233−31245

AUTHOR INFORMATION

Corresponding Author

Yutaka Inoue − *Laboratory of Nutri-Pharmacotherapeutics Management, Faculty of Pharmacy and Pharmaceutical Sciences, Josai University, Sakado, Saitama 3500295, Japan;* orcid.org/0000-0003-3419-343X; Phone: +81-49-271-7980; Email: yinoue@josai.ac.jp; Fax: +81-49-271-7980

Authors

Rino Tachikawa − *Laboratory of Nutri-Pharmacotherapeutics Management, Faculty of Pharmacy and Pharmaceutical Sciences, Josai University, Sakado, Saitama 3500295, Japan*

Hiroki Saito − *Laboratory of Clinical Pharmacology, Faculty of Pharmacy and Pharmaceutical Sciences, Josai University, Sakado, Saitama 3500295, Japan*

Hajime Moteki − *Laboratory of Clinical Pharmacology, Faculty of Pharmacy and Pharmaceutical Sciences, Josai University, Sakado, Saitama 3500295, Japan*

Mitsutoshi Kimura − *Laboratory of Clinical Pharmacology, Faculty of Pharmacy and Pharmaceutical Sciences, Josai University, Sakado, Saitama 3500295, Japan*

Hiroaki Kitagishi − *Department of Molecular Chemistry and Biochemistry, Faculty of Science and Engineering, Doshisha University, Kyotanabe, Kyoto 6100321, Japan;* orcid.org/0000-0003-4682-7217

Florencio Arce, Jr. − *Pharmaceutical Research and Drug Development Laboratories, Department of Pharmacy, School of Health Care Professions, University of San Carlos, Cebu City 6000, The Philippines*

Gerard Lee See − *Pharmaceutical Research and Drug Development Laboratories, Department of Pharmacy, School of Health Care Professions, University of San Carlos, Cebu City 6000, The Philippines*

Takashi Tanikawa − *Laboratory of Nutri-Pharmacotherapeutics Management, Faculty of Pharmacy and Pharmaceutical Sciences, Josai University, Sakado, Saitama 3500295, Japan*

Complete contact information is available at: https://pubs.acs.org/10.1021/acsomega.2c03489

Funding

This research received no external funding.

Notes

The authors declare no competing financial interest.

ACKNOWLEDGMENTS

The authors are grateful to Cyclo Chem Bio Co., Ltd. for providing the cyclodextrin samples.

ABBREVIATIONS

SAC	*S*-allylcysteine
αCD	α-cyclodextrin
βCD	β-cyclodextrin
γCD	γ-cyclodextrin
PM	physical mixture
FD	freeze-drying
ITC	isothermal titration calorimetry
PXRD	powder X-ray diffraction
DSC	differential scanning calorimetry
NIR	near infrared
NOESY	nuclear Overhauser effect spectroscopy
HPLC	high-performance liquid chromatography
HepG2	Hepatocellular Carcinoma
DMEM	Dulbecco's modified Eagle medium
PBS	phosphate-buffered saline

REFERENCES

(1) Fujii, T.; Matsutomo, T.; Kodera, Y. Changes of S-Allylmercaptocysteine and γ-Glutamyl-S-allylmercaptocysteine Contents and Their Putative Production Mechanisms in Garlic Extract during the Aging Process. *J. Agric. Food Chem.* **2018**, *66*, 10506−10512.

(2) Colín-González, A. L.; Ali, S. F.; Túnez, I.; Santamaría, A. On the antioxidant, neuroprotective and anti-inflammatory properties of S-allyl cysteine: An update. *Neurochem. Int.* **2015**, *89*, 83−91.

(3) Gupta, V. B.; Indi, S. S.; Rao, K. S. J. Garlic Extract Exhibits Antiamyloidogenic Activity on Amyloid-beta Fibrillogenesis: Relevance to Alzheimer's Disease. *Phytother Res.* **2009**, *23*, 111−115.

(4) Sohn, C. W.; Kim, H.; You, B. R.; Kim, M. J.; Kim, H. J.; Lee, J. Y.; Sok, D. E.; Kim, J. H.; Lee, K. J.; Kim, M. R. High Temperature- and High Pressure-Processed Garlic Improves Lipid Profiles in Rats Fed High Cholesterol Diets. *J. Med. Food* **2012**, *15*, 435−440.

(5) Agbana, Y. L.; Ni, Y.; Zhou, M.; Zhang, Q.; Kassegne, K.; Karou, S. D.; Kuang, Y.; Zhu, Y. Garlic-derived bioactive compound S-allylcysteine inhibits cancer progression through diverse molecular mechanisms. *Nutr. Res.* **2020**, *73*, 1−14.

(6) Chen, P.; Hu, M.; Liu, F.; Yu, H.; Chen, C. S-allyl-L-cysteine (SAC) protects hepatocytes from alcohol-induced apoptosis. *FEBS Open Bio* **2019**, *9*, 1327−1336.

(7) Rahman, K.; Lowe, G. M. Garlic and Cardiovascular Disease: A Critical Review. *J. Nutr.* **2006**, *136*, 736S−740S.

(8) Brewster, M. E.; Loftsson, T. Cyclodextrins as pharmaceutical solubilizers. *Adv. Drug Deliv. Rev.* **2007**, *59*, 645−666.

(9) Ozdemir, N.; Pola, C. C.; Teixeira, B. N.; Hill, L. E.; Bayrak, A.; Gomes, C. L. Preparation of black pepper oleoresin inclusion complexes based on beta-cyclodextrin for antioxidant and antimicrobial delivery applications using kneading and freeze drying methods: A comparative study. *Lebensm.-Wiss. & Technol.* **2018**, *91*, 439−445.

(10) Zhang, W.; Li, X.; Yu, T.; Yuan, L.; Rao, G.; Li, D.; Mu, C. Preparation, physicochemical characterization and release behavior of the inclusion complex of trans-anethole and β-cyclodextrin. *Food Res. Int.* **2015**, *74*, 55−62.

(11) Ikeda, N.; Inoue, Y.; Ogata, Y.; Murata, I.; Meiyan, X.; Takayama, J.; Sakamoto, T.; Okazaki, M.; Kanamoto, I. Improvement of the Solubility and Evaluation of the Physical Properties of an Inclusion Complex Formed by a New Ferulic Acid Derivative and γ-Cyclodextrin. *ACS Omega* **2020**, *5*, 12073−12080.

(12) Jiang, L.; Yang, J.; Wang, Q.; Ren, L.; Zhou, J. Physicochemical properties of catechin/β-cyclodextrin inclusion complex obtained via co-precipitation. *CyTA—J. Food* **2019**, *17*, 544−551.

(13) Karathanos, V. T.; Mourtzinos, I.; Yannakopoulou, K.; Andrikopoulos, N. K. Study of the solubility, antioxidant activity and structure of inclusion complex of vanillin with β-cyclodextrin. *Food Chem.* **2007**, *101*, 652−658.

(14) Bayomi, M. A.; Abanumay, K. A.; Al-Angary, A. Effect of inclusion complexation with cyclodextrins on photostability of nifedipine in solid-state. *Int. J. Pharm.* **2002**, *243*, 107−117.

(15) Shiozawa, R.; Inoue, Y.; Murata, I.; Kanamoto, I. Effect of antioxidant activity of caffeic acid with cyclodextrins using ground mixture method. *Asian J. Pharm. Sci.* **2018**, *13*, 24−33.

(16) Priya, A. S.; Sivekamavalli, J.; Vaseeharan, B.; Stalin, T. Improvement on dissolution rate of inclusion complex of Rifabutin drug with β-cyclodextrin. *Int. J. Biol. Macromol.* **2013**, *62*, 472−480.

(17) Santos, E. H.; Kamimura, J. A.; Hill, L. E.; Gomes, C. L. Characterization of carvacrol beta-cyclodextrin inclusion complexes as delivery systems for antibacterial and antioxidant applications. *LWT–Food Sci. Technol.* **2015**, *60*, 583−592.

(18) Inoue, Y.; Suzuki, K.; Ezawa, T.; Murata, I.; Yokota, M.; Tokudome, Y.; Kanamoto, I. Examination of the physicochemical

properties of caffeic acid complexed with γ-cyclodextrin. *J. Inclusion Phenom. Macrocyclic Chem.* **2015**, *83*, 289−298.
(19) Pralhad, T.; Rajendrakumar, K. Study of freeze-dried quercetin−cyclodextrin binary systems by DSC, FT-IR, X-ray diffraction and SEM analysis. *J. Pharm. Biomed. Anal.* **2004**, *34*, 333−339.
(20) Nisar, T.; Wang, Z. C.; Yang, X.; Tian, Y.; Iqbal, M.; Guo, Y. Characterization of citrus pectin films integrated with clove bud essential oil: Physical, thermal, barrier, antioxidant and antibacterial properties. *Int. J. Biol. Macromol.* **2018**, *106*, 670−680.
(21) Ogata, Y.; Inoue, Y.; Ikeda, N.; Murata, I.; Kanamoto, I. Improvement of stability due to a cyclamen aldehyde/β-cyclodextrin inclusion complex. *J. Mol. Struct.* **2020**, *1215*, 128161.
(22) Kodera, Y.; Suzuki, A.; Imada, O.; Kasuga, S.; Sumioka, I.; Kanezawa, A.; Taru, N.; Fujikawa, M.; Nagae, S.; Masamoto, K.; Maeshige, K.; Ono, K. Physical, Chemical, and Biological Properties of S-Allylcysteine, an Amino Acid Derived from Garlic. *J. Agric. Food Chem.* **2002**, *50*, 622−632.
(23) Nguyen, T. V. A.; Yoshii, H. Release behavior of allyl sulfide from cyclodextrin inclusion complex of allyl sulfide under different storage conditions. *Biosci. Biotechnol. Biochem.* **2018**, *82*, 848−855.
(24) Inoue, Y.; Yoshida, M.; Ezawa, T.; Tanikawa, T.; Arce, F. J.; See, G. L.; Tomita, J.; Suzuki, M.; Oguchi, T. Inclusion Complexes of Daidzein with Cyclodextrin-Based Metal-Organic Framework-1 Enhance Its Solubility and Antioxidant Capacity. *AAPS PharmSciTech* **2022**, *23*, 2.
(25) Lis-Cieplak, A.; Sitkowski, J.; Kolodziejski, W. Comparative Proton Nuclear Magnetic Resonance Studies of Amantadine Complexes Formed in Aqueous Solutions with Three Major Cyclodextrins. *J. Pharm. Sci.* **2014**, *103*, 274−282.
(26) Choi, S. N.; Ullah, H. M.; Hong, I. H.; Park, J. K.; Park, S.; Chung, M. J.; Son, J. Y.; Yun, H. H.; Yim, J. H.; Jung, S. J.; Chung, H. Y.; Jeong, K. S. Hepatic Protective Effects of S-Allyl-L-Cysteine (SAC) in Rats with Carbon Tetrachloride (CCl4) Induced Liver Injury. *Food Sci. Nutr.* **2020**, *11*, 1053−1069.
(27) Zhao, M. X.; Ji, L. N.; Mao, Z. W. β-Cyclodextrin/Glycyrrhizic Acid Functionalised Quantum Dots Selectively Enter Hepatic Cells and Induce Apoptosis. *Chemistry* **2012**, *18*, 1650−1658.
(28) Cerella, C.; Dicato, M.; Jacob, C.; Diederich, M. Chemical Properties and Mechanisms Determining the Anti-Cancer Action of Garlic-Derived Organic Sulfur Compounds. *Anti-Cancer Agents Med. Chem.* **2011**, *11*, 267.

https://doi.org/10.1021/acsomega.2c03489
ACS Omega 2022, 7, 31233−31245